J Mol Model (2011) 17:59–72
DOI 10.1007/s00894-010-0699-3

ORIGINAL PAPER

Urocanic acid as an efficient hydroxyl radical scavenger: a quantum theoretical study

Saumya Tiwari · Phool Chand Mishra

Received: 29 December 2009 / Accepted: 25 February 2010 / Published online: 2 April 2010
© Springer-Verlag 2010

Abstract The photoisomerization of urocanic acid (UCA)—which is present in human skin epidermis, where it acts as a sunscreen—from its *trans* isomer to its *cis* isomer upon exposure to UV-B radiation is known to cause immunosuppression. In recent years, the antioxidant properties of UCA (it acts as a hydroxyl radical scavenger) have also been recognized. In view of this, the mechanisms of stepwise reactions of *trans*-UCA with up to four hydroxyl radicals were investigated. The molecular geometries of the different species and complexes involved in the reactions (reactant, intermediate and product complexes, as well as transition states) were optimized via density functional theory in the gas phase. Solvation in aqueous media was treated with single point energy calculations using DFT and the polarizable continuum model. Single point energy calculations in the gas phase and aqueous media were also carried out using second-order Møller–Plesset perturbation theory (MP2). The AUG-cc-pVDZ basis set was employed in all calculations. Corrections for basis set superposition error (BSSE) were applied. Vibrational frequency analysis was performed for each optimized structure to ensure the validity of the optimized transition states. It was found that the binding of the first OH· radical to UCA involves a positive energy barrier, while subsequent reactions of OH· radicals are exergonic. Transition states were successfully located, even in those cases where the barrier energies were found to be negative. The *cis–trans* isomerization barrier energy of UCA and that of the first OH· radical addition to UCA are comparable, meaning that both processes can occur simultaneously. It was found that UCA could serve as an antioxidant in the form of an efficient OH· radical scavenger.

Keywords Urocanic acid · Antioxidant · OH radical scavenger · Skin cancer

Introduction

Urocanic acid (UCA) is a metabolite of histidine and is present in the upper layers of the human skin epidermis. It is a major absorber of UV radiation [1–4]; it occurs naturally as its *trans* isomer, but can isomerize to its *cis* isomer under UV irradiation [5, 6]. *Trans*-UCA absorbs UV-B radiation strongly and is therefore believed to be a natural sunscreen, protecting against harmful UV rays from the sun [7]. Because of this, and in order to help prevent skin cancer and other skin diseases, UCA has been used as a component of skin lotions [8]. It was proposed that UCA is a mediator of UV-induced immunosuppression [9]. It has been found in some previous studies that the mechanism of UV-induced immunosuppression involves the formation of *cis*-UCA from *trans*-UCA [10–13]. However, in several in vitro experiments, immunosuppression was not observed [14–18].

The electronic spectrum, the structure and the photoisomerization of UCA have been studied using fluorescence spectroscopy and theoretical methods [19–23]. Simon and coworkers have studied UCA and concluded that its wavelength-dependent photochemistry is due to the involvement of multiple electronic excited states [20–23].

Electronic supplementary material The online version of this article (doi:10.1007/s00894-010-0699-3) contains supplementary material, which is available to authorized users.

S. Tiwari · P. Chand Mishra (✉)
Department of Physics, Banaras Hindu University,
Varanasi 221 005, India
e-mail: pcmishra_in@yahoo.com

Brookman et al. have studied the photophysics and photochemistry of *trans*-UCA and shown that, in buffered aqueous solutions, the *cis* and *trans* forms of UCA exhibit very similar photophysical properties [24]. Wendy et al. performed fluorescence excitation and dispersed emission studies in a supersonic jet to investigate the excited states involved in fluorescence from both the *cis* and *trans* isomers of UCA [25, 26]. Danielsson and Laaksonen theoretically investigated the gas-phase photoisomerization of urocanic acid using time-dependent density functional theory, and estimated the *trans* to *cis* isomerization barrier energy to be more than 20 kcal mol^{-1} [27].

It is observed that, upon exposure to UV-B radiation, *trans*-UCA is not only photoisomerized to *cis*-UCA, but it is also photooxidized [28–30]. Elton and Morrison have observed that the irradiation of UCA with monochromatic light produces singlet oxygen [29]. They have also reported that UCA is a hydroxyl radical scavenger and thus plays an important role as an antioxidant [29]. The primary oxidation products of UCA have been identified as imidazole-4-carboxaldehyde (ImCHO) and glyoxylic acid (GLX) [26], and ImCHO is rapidly oxidized further to imidazole-4-carboxylic acid (ImCOOH) [28]. There is strong experimental evidence that exposure of the skin to UV radiation enhances oxidative stress due to the increased formation of hydroxyl radicals [31–37]. Hydroxyl radicals can also be generated from hydrogen peroxide upon UV irradiation or due to the catalytic involvement of metal ions such as the ferrous (Fe^{2+}) ion [33, 35]. Both of these types of mechanisms can operate in the skin epidermis [30].

Kammeyer et al. have shown that UCA is a good hydroxyl radical scavenger that serves as an antioxidant for the skin [28]. They proposed that the presence of the acrylic acid moiety in UCA conjugated with the imidazole ring may be responsible for its increased scavenging ability towards hydroxyl radicals as compared to those of other 4-(5-)substituted imidazole derivatives [28]. It was suggested that UCA would be more effective as an antioxidant than vitamin E, as it easily dissolves in aqueous solution, whereas vitamin E is only partially soluble in water [28]. As UCA is a natural component of biological systems and is essentially nontoxic, its use in food or cosmetic products is advantageous and convenient [8].

The oxidation of UCA and the formation of oxidative products due to its reaction with OH· radicals have been studied experimentally [28]. However, no theoretical study has been reported on the scavenging action of UCA for OH· radicals and the corresponding mechanisms of formation of the oxidative products. Therefore, we have studied this aspect, and the results we obtained are presented here. The reactions of OH· radicals with other molecules and the properties of antioxidants and other biomolecules have been studied previously [38–40].

Computational details

The molecular geometries of the *cis* and *trans* isomers of UCA and that of the OH· radical were optimized using density functional theory at the B3LYP/AUG-cc-pVDZ and BHandHLYP/AUG-cc-pVDZ levels in the gas phase [41–44]. The geometries of the transition states and adducts involved in the addition reaction of an OH· radical at the C2, C4, C5, C6, C7 and C8 positions of UCA were obtained at these two levels of theory (Fig. 1). The equilibrium geometries of the products and those of the transition states involved in the reaction of another OH· radical with each of the adducts obtained after the addition of one OH· radical to UCA, leading to the formation of different products, were also optimized at these two levels of theory. A third OH· radical was allowed to react with the most stable product formed due to the reaction of the second OH· radical. This reaction could proceed in two different ways, both of which were studied. The fourth OH· radical was allowed to react with each of the two products obtained after the reaction of the third OH· radical. The primary reaction product thus obtained was also observed experimentally. The barrier energies involved in the reactions of one to four OH· radicals were calculated at the BHandHLYP/AUG-cc-pVDZ and MP2/AUG-cc-pVDZ levels of theory in the gas phase and in aqueous media with respect to the corresponding sums of the total energies of the isolated reactants.

The geometry optimization calculations were performed at the B3LYP/AUG-cc-pVDZ and BHandHLYP/AUG-cc-pVDZ levels of theory in the gas phase. The structures optimized at these levels of theory were solvated in bulk aqueous media using single point energy calculations at the corresponding levels of theory employing the polarizable continuum model (PCM) [45–48]. In the PCM, a cavity is considered to be formed by interlocking spheres of radii 1.2 times the van der Waals radii of the atoms of the solute molecule. Single point energy calculations were also performed in both the gas phase and aqueous media at the MP2/AUG-cc-pVDZ level of theory [49–53] using the geometries optimized at the BHandHLYP/AUG-cc-pVDZ level in gas phase, where the PCM was used for the calculations in aqueous media.

Vibrational frequency analysis was carried out for each optimized structure at the same level of theory at which geometry optimization was performed in the gas phase, in order to ensure that each total energy extremum investigated was genuine, each minimum had all real frequencies, and each transition state had only one imaginary frequency. The validity of the transition states was ensured by visually examining the vibrational modes corresponding to the imaginary frequencies and applying the condition that these should connect the reactant and product complexes properly. As the validity of the optimized transition states was obvious, intrinsic reaction coordinate (IRC) calculations were not performed for this

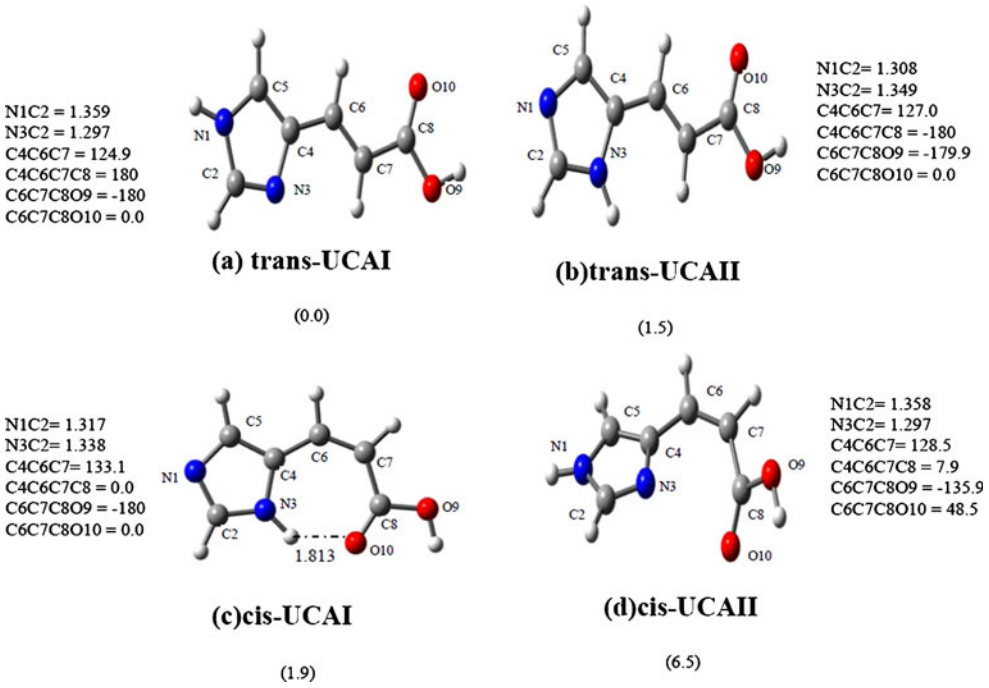

Fig. 1 Two tautomers of *trans*-UCA (**a**, **b**) and two tautomers of *cis*-UCA (**c**, **d**). The relative ZPE-corrected total energies (kcal mol^{-1}) of **a**–**d** obtained in aqueous media at the MP2/AUG-cc-pVDZ level of theory using the geometries optimized at the BHandHLYP/AUG-cc-pVDZ level in the gas phase are given with respect to that of **a**

purpose. Gibbs free energies at 298.15 K and zero-point energy (ZPE)-corrected total energies were obtained in each case at the B3LYP/AUG-cc-pVDZ and BHandHLYP/AUG-cc-pVDZ levels of theory in the gas phase. As an approximation, ZPE corrections and thermal energy corrections giving Gibbs free energies obtained at the BHandHLYP/AUG-cc-pVDZ level were also applied to the total energies obtained by single point energy calculations at the MP2/AUG-cc-pVDZ level of theory in both the gas phase and aqueous media. Corrections for basis-set superposition error (BSSE) obtained by single point energy calculations in the gas phase and aqueous media at the BHandHLYP/AUG-cc-pVDZ level of theory using the counterpoise method were obtained [51, 52]. Further, as an approximation, the BSSE corrections obtained at the BHandHLYP/AUG-cc-pVDZ level were also applied to the total energies obtained at the single point MP2/AUG-cc-pVDZ level. All of the calculations were carried out using the Windows version of the Gaussian 98 (G98W) suite of

Table 1 Relative ZPE-corrected total energies (kcal mol^{-1}) of *trans* and *cis* isomers of the N1H and N3H tautomers of UCA obtained at different levels of theory in the gas phase and aqueous media with respect to the ZPE-corrected total energy of the corresponding most stable structure[a]

Medium and level of theory				
Trans and cis isomers of tautomers of UCA[b]	Relative total energy in gas phase[c]		Relative total energy in aqueous media[d]	
	BHandHLYP/AUG-cc-pVDZ	MP2/AUG- cc-pVDZ	BHandHLYP/ AUG-cc-pVDZ	MP2/AUG- cc-pVDZ
trans-UCAI	3.1	24.5	0.0	0.0
trans-UCAII	3.7	26.3	1.7	1.5
cis-UCAI	0.0	0.0	3.1	1.9
cis-UCAII	12.4	10.6	8.1	6.5

[a] Structures of *trans* and *cis* isomers of the N1H and N3H tautomers of UCA are given in Fig. 1

[b] *Trans*-UCAI, *trans*-UCAII, *cis*-UCAI and cis-UCAII have N1H, N3H, N3H and N1H forms respectively (Fig. 1)

[c] The relative ZPE-corrected total energies of *trans*-UCAI, *trans*-UCAII, *cis*-UCAI and *cis*-UCAII are given with respect to that of *cis*-UCAI at each level of theory

[d] The relative ZPE-corrected total energies of *trans*-UCAI, *trans*-UCAII, *cis*-UCAI and *cis*-UCAII are given with respect to that of *trans*-UCAI at each level of theory

Table 2 ZPE-corrected barrier energies and the corresponding Gibbs free energy changes (kcal mol^{-1}) involved in the formation of the C_2.OH·, C_4.OH·, C_5.OH·, C_6.OH·, C_7.OH· and C_8.OH· adducts of UCA obtained at the different levels of theory in the gas phase and aqueous media[a]

Sites of UCA[c]	Barrier energies and Gibbs free energy changes	BHandHLYP/ AUG- cc–pVDZ	MP2/AUG-cc-pVDZ[d]
C2	ΔE^b_2	2.9 (6.8)	20.4 (20.5)
	ΔG^b_2	11.4 (15.4)	28.9 (29.0)
C4	ΔE^b_4	9.3 (9.5)	19.1 (15.2)
	ΔG^b_4	18.1 (18.3)	27.9 (23.9)
C5	ΔE^b_5	4.2 (1.0)	17.5 (10.4)
	ΔG^b_5	13.4 (10.4)	26.6 (19.6)
C6	ΔE^b_6	2.9 (6.3)	12.2 (13.5)
	ΔG^b_6	11.8 (14.9)	21.0 (22.1)
C7	ΔE^b_7	1.9 (4.1)	12.4 (14.6)
	ΔG^b_7	10.3 (12.5)	22.2 (22.9)
C8	ΔE^b_8	18.8 (21.7)	31.3 (30.3)
	ΔG^b_8	27.7 (30.6)	40.2 (39.2)

[a] Energies obtained in aqueous media are given in parentheses

[c] Structures of the different adducts are shown in Fig. 2

[d] Single point energy calculations were performed at the MP2/AUG-cc-pVDZ level employing the geometries optimized at the BHandHLYP/AUG-cc-pVDZ level. In aqueous media, single point energy calculations were performed using the PCM

programs [54]. The GaussView program was employed to visualize the optimized structures and vibrational modes [55].

Results and discussion

Structure and stability of UCA

We mainly considered the BSSE-corrected energies obtained by single point energy calculations at the MP2/AUG-cc-pVDZ level in aqueous media employing the gas phase geometries optimized at the BHandHLYP/AUG-cc-pVDZ level and the PCM. This was done because these energies would include both an improved electron correlation treatment and the solvent effect of the medium. Although UCA occurs in the skin epidermis in the zwitterionic or anionic form [56], we have studied its scavenging action towards OH· radicals when it is in its normal neutral form. To study reactions of the zwitterionic form of UCA, one must carry out all of the geometry optimization calculations while accounting for environmental effects, which may be approximated by the solvent effect of water, e.g., by employing the polarizable continuum model (PCM). It did not seem feasible to perform such calculations in aqueous media for all of the reactions studied by us [57, 58]. Due to this reason, we studied the reactions of OH· radicals with the normal neutral form of UCA. One would expect that the results obtained for the normal neutral form of UCA would also be qualitatively applicable to its zwitterionic or anionic form.

The geometries of the *trans* and *cis* isomers of UCA were previously studied by Lahti et al. [59, 60], and other studies have also been performed on the structure and conformational properties of UCA [19, 59-65]. The UV absorption spectrum of UCA is broad, featureless and difficult to interpret unambiguously, which can be ascribed to the presence of several rotamers obtained by rotations about the single bonds in the acrylic acid chain of the molecule [19, 61].

The geometries of the two (N1H, N3H) tautomers of each of *trans*-UCA and *cis*-UCA shown in Fig. 1 were optimized at the BHandHLYP/AUG-cc-pVDZ level of theory in the gas phase. The ZPE-corrected relative total energies of these structures obtained at the MP2/AUG-cc-pVDZ level of theory in aqueous media are given in Fig. 1. Relative ZPE-corrected total energies of both the tautomers of each of the *trans* and *cis* isomers of UCA obtained at the different levels of theory in the gas phase and aqueous media are presented in Table 1. The relative ZPE-corrected total energies (Table 1) show that, in the gas phase, the N3H tautomer of *cis*-UCA (called *cis*-UCAI) is the most stable of the four structures. However, in aqueous media, the N1H tautomer of *trans*-UCA (called *trans*-UCAI) is the most stable of the four structures (Table 1). We also note that, with regard to the relative stabilities of the four structures, the results obtained at the BHandHLYP/AUG-cc-pVDZ and MP2/AUG-cc-pVDZ levels of theory in both the gas phase and aqueous media are qualitatively similar. In *cis*-UCAI, there is an intramolecular hydrogen bond between the NH and CO groups, while no such hydrogen bond is present in any of the other three structures. The conformation of the chain of UCA that has been observed by crystallography is the same as that of *trans*-

Table 3 Binding energies (kcal mol^{-1}) of the adducts C_2.OH·, C_4.OH·, C_5.OH·, C_6.OH·, C_7.OH· and C_8.OH· obtained at different levels of theory in the gas phase and aqueous media[a]

Adducts[b]	BHandHLYP/AUG-cc-pVDZ	MP2/ AUG- cc-pVDZ[c]
C_2.OH·	−20.9 (−19.8)	−4.3 (−10.9)
C_4.OH·	−6.9 (−2.5)	−7.6 (−8.6)
C_5.OH·	−26.9 (−28.3)	−14.4 (−19.5)
C_6.OH·	−23.7 (−19.0)	−27.7 (−24.8)
C_7.OH·	−27.5 (−24.3)	−23.2 (−23.0)
C_8.OH·	2.7 (4.3)	16.3 (25.5)

[a] Binding energies obtained in aqueous media are given in parentheses.

[b] Structures of the different adducts are shown in Fig. 2.

[c] Single point energy calculations were performed at the MP2/AUG-cc-pVDZ level employing the geometries optimized at the BHandHLYP/AUG-cc-pVDZ level. In aqueous media, single point energy calculations were performed using the PCM

Table 4 ZPE-corrected barrier energies and the corresponding Gibbs free energy changes (kcal mol^{-1}) involved in the reactions of the second OH· radical with the adducts C_5.OH· , C_6.OH· and C_7.OH· at their various sites obtained at different levels of theory in the gas phase and aqueous media[a]

Barrier energies and Gibbs free energy changes[c]	BHandHLYP/ AUG-cc–pVDZ	MP2/AUG-cc-pVDZ[d]
$\Delta E^{b}_{5,2}$	−24.5 (−16.0)	−55.9 (−38.1)
$\Delta G^{b}_{5,2}$	−6.5 (−1.9)	−26.7 (−20.2)
$\Delta E^{b}_{5,4}$	−47.8 (−45.5)	−81.5 (−69.3)
$\Delta G^{b}_{5,4}$	−28.6 (−27.3)	−51.0 (−50.1)
$\Delta E^{b}_{5,6}$	−26.0 (−27.4)	−45.2 (−56.6)
$\Delta G^{b}_{5,6}$	−6.6 (−15.3)	−25.7 (−37.2)
$\Delta E^{b}_{5,7}$	−30.7 (−28.6)	−64.8 (−54.2)
$\Delta G^{b}_{5,7}$	−11.4 (−9.3)	−34.1 (−34.9)
$\Delta E^{b}_{6,2}$	−35.2 (−34.7)	−60.5 (−48.0)
$\Delta G^{b}_{6,2}$	4.5 (−28.0)	−30.6 (−55.2)
$\Delta E^{b}_{6,4}$	4.5 (−28.0)	−30.6 (−55.2)
$\Delta G^{b}_{6,4}$	23.7 (−8.9)	−0.2 (−36.1)
$\Delta E^{b}_{6,5}$	−29.2 (−26.6)	−63.7 (−50.4)
$\Delta G^{b}_{6,5}$	−10.1 (−7.4)	−30.9 (−31.4)
$\Delta E^{b}_{6,7}$	−19.6 (−21.5)	−61.6 (−49.5)
$\Delta G^{b}_{6,7}$	−0.6 (−2.5)	−25.3 (−30.5)
$\Delta E^{b}_{7,2}$	−20.7 (−20.5)	−56.6 (−46.4)
$\Delta G^{b}_{7,2}$	−2.3 (−2.1)	−26.9 (−28.0)
$\Delta E^{b}_{7,4}$	−7.2 (−9.4)	−50.5 (−41.5)
$\Delta G^{b}_{7,4}$	−11.3 (−8.7)	−20.5 (−23.0)
$\Delta E^{b}_{7,5}$	−22.5 (−22.5)	−54.5 (−46.1)
$\Delta G^{b}_{7,5}$	−5.2 (−5.3)	−25.8 (−28.8)
$\Delta E^{b}_{7,6}$	−34.6 (−40.5)	−65.6 (−63.2)
$\Delta G^{b}_{7,6}$	−16.4 (−22.3)	−36.0 (−44.9)

[a] Energies obtained in aqueous media are given in parentheses

[c] Structures of the different structures are shown in Figs. 3 as well as Figs. SI1, SI2 and SI3 in the "Electronic supplementary material". The first subscript represents the site where an OH group is already bonded, while the second subscript represents the site at which the second OH group is attached in the reaction under consideration

[d] Single point energy calculations were performed at the MP2/AUG-cc-pVDZ level employing the geometries optimized at the BHandHLYP/AUG-cc-pVDZ level. In aqueous media, single point energy calculations were performed using the PCM

UCAI, except that the observed structure is zwitterionic [66]. In view of the highest stability of *trans*-UCAI in aqueous media, reactions of OH· radicals with this species, hereafter simply referred to as UCA, were studied. However, we would expect to get similar results even if we considered *cis*-UCAI instead of *trans*-UCAI.

Reactions of one OH· radical with UCA

We will consider addition reactions of an OH· radical at the different sites of UCA. In the following reaction, let us represent UCA simply as C_n, which implies that the addition of an OH· radical will occur at the site C_n in UCA. Then,

$$C_n + OH^{\cdot} \xrightarrow{\Delta E_n^b} [TS]_n \xrightarrow{-\Delta E_n^r} C_n{\cdot}OH^{\cdot} \quad (1)$$

where n=2, 4, 5, 6, 7 and 8 are the different carbon atoms of UCA (Fig. 1), $\Delta E_n{}^b$ is the barrier energy of the addition reaction of an OH· radical at the C_n site, while $\Delta E_n{}^r$ is the corresponding released energy. $[TS]_n$ is the transition state involved in the reaction at the C_n site.

The ZPE- and BSSE-corrected barrier energies and the corresponding Gibbs free energy changes involved in the addition of an OH· radical at the C2, C4, C5, C6, C7 or C8 position of UCA are given in Table 2. The barrier energies were also calculated at the B3LYP/AUG-cc-pVDZ level of theory in the gas phase and aqueous media, followed by single point energy calculations at the MP2/AUG-cc-pVDZ level. The corresponding B3LYP/AUG-cc-pVDZ and MP2/AUG-cc-pVDZ results were found to be very different. In particular, the barrier energies obtained at the former level were found to be much less than those obtained at the latter level. Such an anomaly was not observed between the results obtained at the BHandHLYP/AUG-cc-pVDZ and MP2/AUG-cc-pVDZ levels. In view of this fact, the B3LYP/AUG-cc-pVDZ results are not presented here. It

Table 5 ZPE-corrected binding energies (kcal mol^{-1}) of the adducts or complex obtained after the reactions of two OH· radicals with UCA at different levels of theory in the gas phase and aqueous media[a]

Adduct or complex[b]	BHandHLYP/ AUG-c c-pVDZ[c]	MP2/ AUG-cc-pVDZ[d]
$C_{5,2}$.2OH·	−80.4 (−76.3)	−108.5 (−95.5)
$C_{5,4}$.2OH·	−85.6 (−77.5)	−113.1 (−98.0)
$C_{5,6}$.2OH·	−74.5 (−67.0)	−107.6 (−92.2)
$C_{5,7}$.2OH·	−80.2 (−77.6)	−108.8 (−96.5)
$C_{6,2}$.2OH·	−21.1 (−34.5)	−45.8 (−56.1)
$C_{6,4}$[e]	−95.3 (−79.8)	−119.1 (−61.5)
$C_{6,5}$.2OH·	−74.5 (−67.0)	−107.6 (−92.2)
$C_{6,7}$.2OH·	−95.8 (−91.6)	−130.0 (−114.1)
$C_{7,2}$.2OH·	−50.5 (−51.7)	−81.6 (−73.9)
$C_{7,4}$.2OH·	−51.5 (−29.6)	−72.1 (−64.4)
$C_{7,5}$.2OH·	−80.1 (−77.4)	−108.8 (−96.5)
$C_{7,6}$.2OH·	−95.8 (−91.6)	−130.0 (−114.1)

[a] Energies obtained in aqueous media are given in parentheses

[b] Structures of the different structures are shown in Figs. 3 as well as Figs. SI1, SI2 and SI3 of the "Electronic supplementary material"

[c] Single point energy calculations were performed at the MP2/AUG-cc-pVDZ level employing the geometries optimized at the BHandHLYP/AUG-cc-pVDZ level. In aqueous media, single point energy calculations were performed using the PCM

[d] In this case, the product is a complex of ImOH and C_2H_3COOH-OH· (see Fig. SI2 in the "Electronic supplementary material")

$$UCA_{6,7}.2OH + OH^{\cdot} \xrightarrow{\Delta E^{b}_{6,7,3,1}} [TS1] \xrightarrow{-\Delta E^{r}_{6,7,3,1}} IC\ (ImCHO + GLXH + H_2O)$$

$$IC + OH^{\cdot} \xrightarrow{\Delta E^{b}_{6,7,4,1}} [TS2] \xrightarrow{-\Delta E^{r}_{6,7,4,1}} PC\ (ImCHO + GLX + 2H_2O)$$

Scheme 1 $UCA_{6,7}.2OH + OH^{\cdot} \xrightarrow{\Delta E_{6,7,3,1}{}^{b}} [TS1] \xrightarrow{-\Delta E_{6,7,3,1}{}^{r}} IC(ImCHO + GLXH + H_2O) IC + OH^{\cdot} \xrightarrow{\Delta E_{6,7,4,1}{}^{b}} [TS2] \xrightarrow{-\Delta E_{6,7,4,1}{}^{r}} PC(ImCHO + GLX + 2H_2O)$

has also been reported in previous studies that the B3LYP method underestimates reaction barrier energies for open shell systems [67–71]. Further, it has been found in some previous studies that the BHandHLYP functional is more reliable than the B3LYP functional for open shell systems [68]. Due to this reason, BSSE-corrected results were obtained using the BHandHLYP functional and the MP2 method only.

At the MP2/AUG-cc-pVDZ level of theory in the gas phase, the ZPE-corrected barrier energies with BSSE correction for OH· radical additions at the C2, C4, C5, C6, C7 and C8 positions of UCA ($\Delta E^{b}{}_2$, $\Delta E^{b}{}_4$, $\Delta E^{b}{}_5$, $\Delta E^{b}{}_6$, $\Delta E^{b}{}_7$ and $\Delta E^{b}{}_8$) were found to be 20.4, 19.1, 17.5, 12.2, 12.4 and 31.3 kcal mol^{-1}, respectively, while in aqueous media, the corresponding barrier energies were found to be 20.5, 15.2, 10.4, 13.5, 14.6 and 30.3 kcal mol^{-1}. The corresponding BSSE-corrected Gibbs free energy changes ($\Delta G^{b}{}_2$, $\Delta G^{b}{}_4$, $\Delta G^{b}{}_5$, $\Delta G^{b}{}_6$, $\Delta G^{b}{}_7$ and $\Delta G^{b}{}_8$) for OH· radical additions at the C2, C4, C5, C6, C7 and C8 positions of UCA in the gas phase at the MP2/AUG-cc-pVDZ level of theory were found to be 28.9, 27.9, 26.6, 21.0, 22.2 and 40.2 kcal mol^{-1}, respectively, while the corresponding energy values in aqueous media were 29.0, 23.9, 19.6, 22.1, 22.9 and 39.2 kcal mol^{-1} (Table 2). We found that the Gibbs free energy changes for the addition reactions mentioned above obtained at the MP2/AUG-cc-pVDZ level of theory in the gas phase or aqueous media were larger than the corresponding ZPE-corrected barrier energies, by 8.9 kcal mol^{-1} on average (Table 2). Such large differences between the ZPE-corrected barrier energies and the corresponding Gibbs free energy changes have also been reported in other studies [72]. At the MP2/AUG-cc-pVDZ level of theory, the ZPE-corrected barrier energies with BSSE correction as well as the corresponding Gibbs free energy changes follow the order C8 > C2 > C4 > C5 > C7 > C6 in gas phase, whereas the corresponding order in aqueous media is C8 > C2 > C4 > C7 > C6 > C5 (Table 2).

The calculated binding energies of the different C_n.OH· adducts (binding energy of an adduct = BSSE-corrected total energy of the adduct − sum of total energies of the reactants) are presented in Table 3. At the MP2/AUG-cc-pVDZ level of theory, the magnitudes of the binding energies follow the order C6 > C7 > C5 > C4 > C2 > C8 in the gas phase, whereas the corresponding order in aqueous media is C6 > C7 > C5 > C2 > C4 > C8 (Table 3). Thus, the adduct C_6.OH· is predicted to be the most stable, with the next most stable adduct being C_7.OH·. If one considers the binding energies and the abovementioned barrier energies, the formation of adducts with an OH· radical at the C6 and C7 sites of the acrylic chain and the C5 position of the imidazole ring of UCA should be most favored. Therefore, these adducts would be the most abundant ones available for the addition reaction of a second OH· radical. The positive binding energy for the C_8.OH· adduct (Table 3) shows that the addition reaction of an OH· radical at the C8 position would not be favored.

Reactions of two OH radicals with UCA adducts (C_n.OH· where n=5, 6, 7)

In accordance with the above discussion, reactions of the second OH· radical with the C_5.OH·, C_6.OH· and C_7.OH· adducts of UCA were allowed to take place. When the second OH· radical reacts with the C_n.OH· adducts at different sites (n=5, 6, 7), the reaction can be described as follows (m represents the site of addition of the second OH· radical):

$$C_n.OH^{\cdot} + OH^{\cdot} \xrightarrow{\Delta E^{b}_{n,m}} [TS]_{n,m} \xrightarrow{-\Delta E^{r}_{n,m}} C_{n,m}.2OH \qquad (2)$$

Here, when n=5, m=2, 4, 6, 7; when n=6, m=2, 4, 5, 7; and when n=7, m=2, 4, 5, 6. When n=6 and m=4, the product is a complex between two radicals; i.e., Im-OH· and C_2H_3COOH-OH·.

The ZPE-and BSSE-corrected barrier energies and the corresponding Gibbs free energy changes for the reactions of the second OH· radical with each of the adducts C_5.OH·, C_6.OH·, and C_7.OH· obtained at the BHandHLYP/AUG-cc-pVDZ and MP2/AUG-cc-pVDZ levels of theory in the gas phase and aqueous media are presented in Table 4. The ZPE- and BSSE-corrected barrier energies and the corresponding Gibbs free energy changes, obtained at the abovementioned level of theory in the gas phase and

$$UCA_{6,7}.2OH + OH^{\cdot} \xrightarrow{\Delta E^{b}_{6,7,3,2}} [TS1'] \xrightarrow{-\Delta E^{r}_{6,7,3,2}} IC'\ (ImCHOH + GLX + H_2O)$$

$$IC' + OH^{\cdot} \xrightarrow{\Delta E^{b}_{6,7,4,2}} [TS2'] \xrightarrow{-\Delta E^{r}_{6,7,4,2}} PC'\ (ImCHO + GLX + 2H_2O)$$

Scheme 2 $UCA_{6,7}.2OH + OH^{\cdot} \xrightarrow{\Delta E_{6,7,3,2}{}^{b}} [TS1'] \xrightarrow{-\Delta E_{6,7,3,2}{}^{r}} IC'(ImCHOH + GLX + H_2O) IC' + OH^{\cdot} \xrightarrow{\Delta E_{6,7,4,2}{}^{b}} [TS2'] \xrightarrow{-\Delta E_{6,7,4,2}{}^{r}} PC'(ImCHO + GLX + 2H_2O)$

Table 6 ZPE-corrected barrier energies (kcal mol^{-1}) of the reactions of the third and fourth OH· radicals, one after the other, with the adduct $C_{6,7}$.2OH· at different levels of theory in the gas phase and aqueous media (see also Schemes 1 and 2)[a]

Schemes, barrier energies and Gibbs free energy changes[c]	BHandHLYP/ AUG-cc-pVDZ	MP2/AUG-cc-pVDZ[d]
Scheme 1		
$\Delta E^{b}_{6,7,3,1}$	−88.5 (−76.3)	−129.7 (−105.2)
$\Delta G^{b}_{6,7,3,1}$	−61.2 (−49.0)	−102.2 (−77.9)
$\Delta E^{b}_{6,7,4,1}$[f]	−159.8 (−142.5)	−206.6 (−190.1)
$\Delta G^{b}_{6,7,4,1}$[f]	−124.7 (−107.5)	−171.6 (−155.1)
Scheme 2		
$\Delta E^{b}_{6,7,3,2}$	−85.3 (−66.7)	−117.1 (−100.5)
$\Delta G^{b}_{6,7,3,2}$	−57.8 (−39.2)	−89.8 (−72.9)
$\Delta E^{b}_{6,7,4,2}$	−183.2 (−164.1)	−231.3 (−211.5)
$\Delta G^{b}_{6,7,4,2}$	−148.3 (−127.0)	−194.2 (−174.4)

[a] Energies obtained in aqueous media are given in parentheses

[c] The different structures are shown in Fig. 4. For an explanation of the subscripts used, see text

[d] Single point energy calculations were performed at the MP2/AUG-cc-pVDZ level employing geometries optimized at the BHandHLYP/AUG-cc-pVDZ level. In aqueous media, single point energy calculations were performed using the PCM

[f] $\Delta E_{6,7,4,1}{}^{b}$ and $\Delta G_{6,7,4,1}$ are not BSSE-corrected due to lack of convergence of BSSE calculations

aqueous media with BSSE correction, are all negative except for one case where the barrier energy and the corresponding Gibbs free energy change are positive in gas phase at the BHandHLYP/AUG-cc-pVDZ level of theory (Table 4). As the barrier energies and the Gibbs free energy changes of the addition reactions are all negative in aqueous media, the corresponding reactions would be barrierless.

The addition reactions of an OH· radical at the C2, C4, C6 and C7 positions of C_5.OH· are shown in Fig. SI1, while the corresponding reactions at the C2, C4 and C5 positions of each of C_6.OH· and C_7.OH· are shown in Figs. SI2 and SI3 in the "Electronic supplementary material". Two interesting cases of the addition an OH· radical to C_6.OH· and C_7.OH· are presented in Figs. 3a, b respectively. In each case, due to abstraction of the hydrogen atom of the first OH group by the second OH group, a transient oxo derivative of UCA complexed with a water molecule is formed in the transition state (Fig. 3a, b). However, during the subsequent step, the water molecule is dissociated into an OH group and a hydrogen atom, and the dissociated hydrogen atom gets bonded to the oxo atom while the dissociated OH group gets bonded to the neighboring carbon atom (C6 or C7). Thus, we get a derivative of UCA as the product, the C6 and C7 atoms of which each have an attached OH group (Fig. 3a, b).

The binding energies of the different complexes and adducts formed after the reaction of the second OH· radical are presented in Table 5. The magnitudes of the binding energies obtained at the MP2/AUG-cc-pVDZ level of theory in aqueous media follow the order $C_{6,7}$.2OH·= $C_{7,6}$.2OH·>$C_{5,4}$.2OH·>$C_{5,7}$.2OH·=$C_{7,5}$.2OH·>$C_{5,2}$.2OH·= $C_{5,6}$.2OH·=$C_{6,5}$.2OH·>$C_{7,2}$.2OH·>$C_{7,4}$.2OH·>ImOH+ C_2H_3COOH-OH·>$C_{6,2}$.2OH·. Among the different complexes and products, $C_{6,7}$.2OH· and $C_{7,6}$.2OH· have the highest binding energies by some degree. In view of this result, a study of reactions of the third and fourth OH· radicals with UCA was performed, considering $C_{6,7}$.2OH· as a reactant.

Reactions of third and fourth OH radicals with $UCA_{6,7}$.2OH·

In accordance with the above discussion, reactions of two OH· radicals with $UCA_{6,7}$.2OH·, one after the other, were allowed to take place. It was found that these reactions could proceed in two different ways, as shown in Schemes 1 and 2 in Fig. 4. These two schemes can also be described as follows:

In the above reactions, the subscripts associated with the barrier and released energies are written as 6, 7, n1, and n2, where n1 stands for the total number of OH· radicals involved in the reaction (3 or 4), while n2 represents the scheme number (1 or 2); the subscripts 6 and 7 represent the sites at which the OH groups are attached. In Scheme 1, the third OH· radical abstracts the hydrogen atom of the OH group attached to the C6 position of the acrylic chain, while in Scheme 2 the third OH· radical abstracts the hydrogen atom of the OH group attached to the C7 position of the same chain. In Scheme 1, GLXH stands for glyoxylic acid with one extra hydrogen atom attached to one of its oxygen atoms (H12 attached to O12, Fig. 4). In Scheme 2, ImCHOH stands for imidazole-4-carboxaldehyde with one extra hydrogen atom attached to its oxygen atom (H11 attached to O11, Fig. 4).

In Scheme 1, after the reaction of the third OH· radical, an intermediate complex (IC) that is a hydrogen-bonded complex of ImCHO, GLXH and H_2O is initially formed. Subsequently, when the fourth OH· radical reacts with the IC, the product complex (PC), which is a hydrogen-bonded complex of ImCHO, GLX and $2H_2O$, is formed. In Scheme 2, an intermediate complex (IC′) that is a hydrogen-bonded complex of ImCHOH, GLX and a water molecule is formed. The final product is the same in both Scheme 1 and Scheme 2. As the same primary reaction product has also been observed experimentally [28], the schemes for the reactions of OH· radicals with UCA considered here appear to simulate the experimental observations satisfactorily. The formation of secondary products due to the reactions of each of ImCHO and GLX with OH·

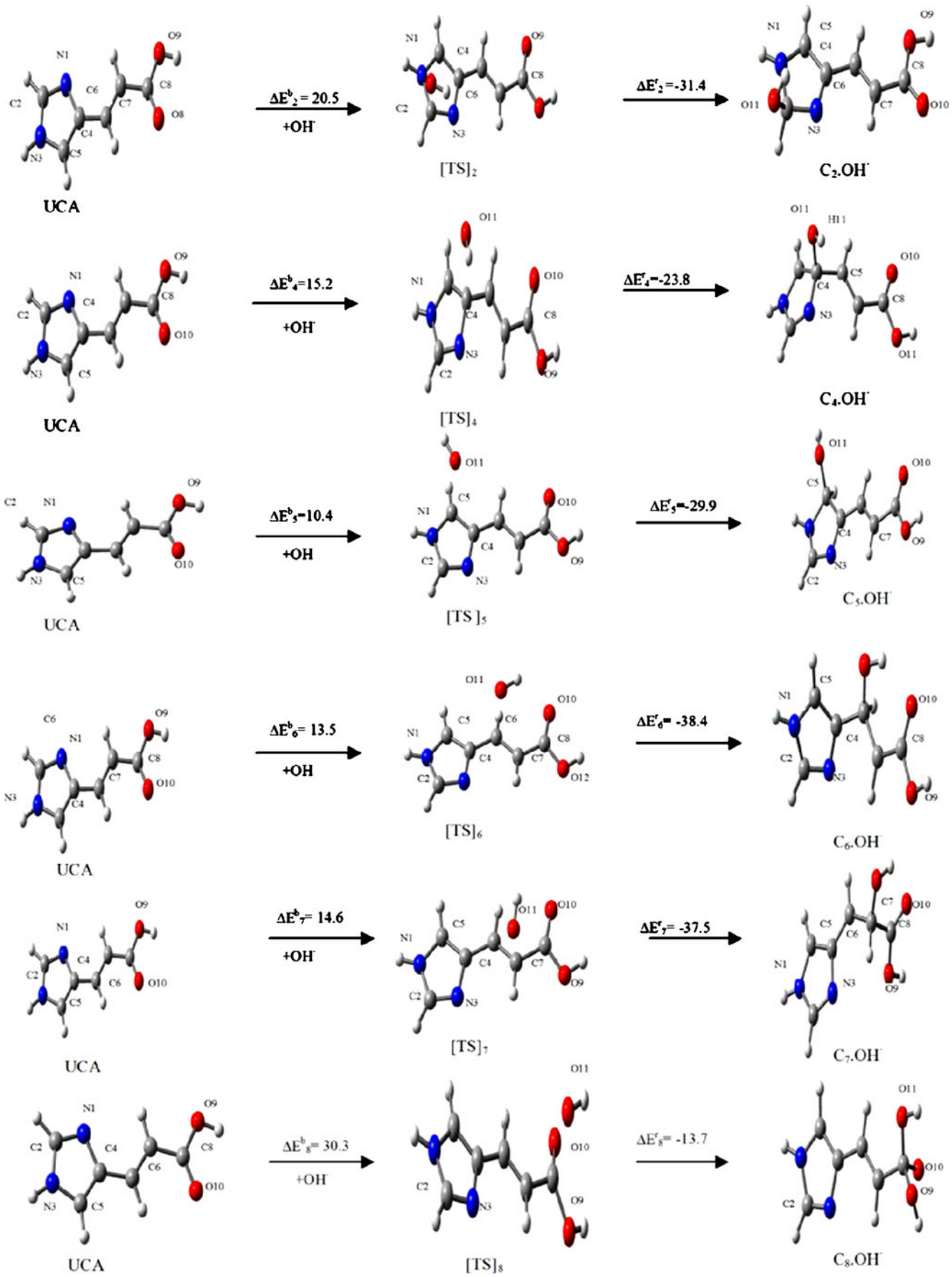
UCA
ΔE^b_2 = 20.5
+OH^-
[TS]_2
ΔE^r_2 = -31.4
C_2.OH^-
UCA
ΔE^b_4 = 15.2
+OH^-
[TS]_4
ΔE^r_4 = -23.8
C_4.OH^-
UCA
ΔE^b_5 = -10.4
+OH
[TS]_5
ΔE^r_5 = -29.9
C_5.OH^-
UCA
ΔE^b_6 = 13.5
+OH
[TS]_6
ΔE^r_6 = -38.4
C_6.OH^-
UCA
ΔE^b_7 = 14.6
+OH^-
[TS]_7
ΔE^r_7 = -37.5
C_7.OH^-
UCA
ΔE^b_8 = 30.3
+OH^-
[TS]_8
ΔE^r_8 = -13.7
C_8.OH^-

◀ **Fig. 2** Addition reactions of an OH· radical at each of the C2, C4, C5, C6 and C7 sites of urocanic acid. ZPE- and BSSE-corrected barrier and released energies (kcal mol^{-1}) obtained in aqueous media at the MP2/AUG-cc-pVDZ level of theory using the geometries optimized at the BHandHLYP/AUG-cc-pVDZ level in the gas phase are given near the *arrows*

radicals can be also occur, as observed experimentally [28, 73]. These reactions can easily be studied theoretically.

The calculated ZPE-corrected barrier energies ($\Delta E^{b}_{6,7,3,1}$, $\Delta E^{b}_{6,7,3,2}$, $\Delta E^{b}_{6,7,4,1}$, $\Delta E^{b}_{6,7,4,2}$) and the corresponding Gibbs free energy changes involved in the reactions of the third and fourth OH· radicals, one after the other, at the different levels of theory in the gas phase and aqueous media are presented in Table 6. These energies, except for $\Delta E^{b}_{6,7,4,1}$ and $\Delta G^{b}_{6,7,4,1}$, are BSSE-corrected. The values of $\Delta E^{b}_{6,7,4,1}$ and $\Delta G^{b}_{6,7,4,1}$ presented in Table 6 are not BSSE-corrected, as convergence was not achieved in the BSSE calculations corresponding to these energies at the BHandHLYP/AUG-cc-pVDZ level. The ZPE-corrected barrier energies ($\Delta E^{b}_{6,7,4,1}$, $\Delta E^{b}_{6,7,4,2}$) involved in the reactions of the fourth OH· radical are highly negative (approximately −200 kcal mol^{-1}) (Fig. 4, Table 6). To understand the reason for such highly negative barrier energies, we must study how the barrier energies change in going from one OH· radical to four OH· radicals, reacting successively. The barrier energies for the addition of the first OH· radical were positive, lying in the range 10 to 30 kcal mol^{-1} (Fig. 2, Table 2), but the barrier energies became negative, ranging from −69 to −38 kcal mol^{-1}, when the second OH· radical reacted (Figs. 3; Figs. SI1, SI2 and SI3, Table 4). In going from two OH· radicals to three, the nature of the reaction changed from one of addition to hydrogen atom abstraction, and the barrier energies became even more negative (approximately −100 kcal mol^{-1}) (Fig. 4, Table 6).

When the fourth OH· radical reacted, the barrier energies almost doubled (i.e., became almost twice as negative) compared to those for the third OH· radical reaction. In the fourth OH· radical reaction, there is OH bond formation

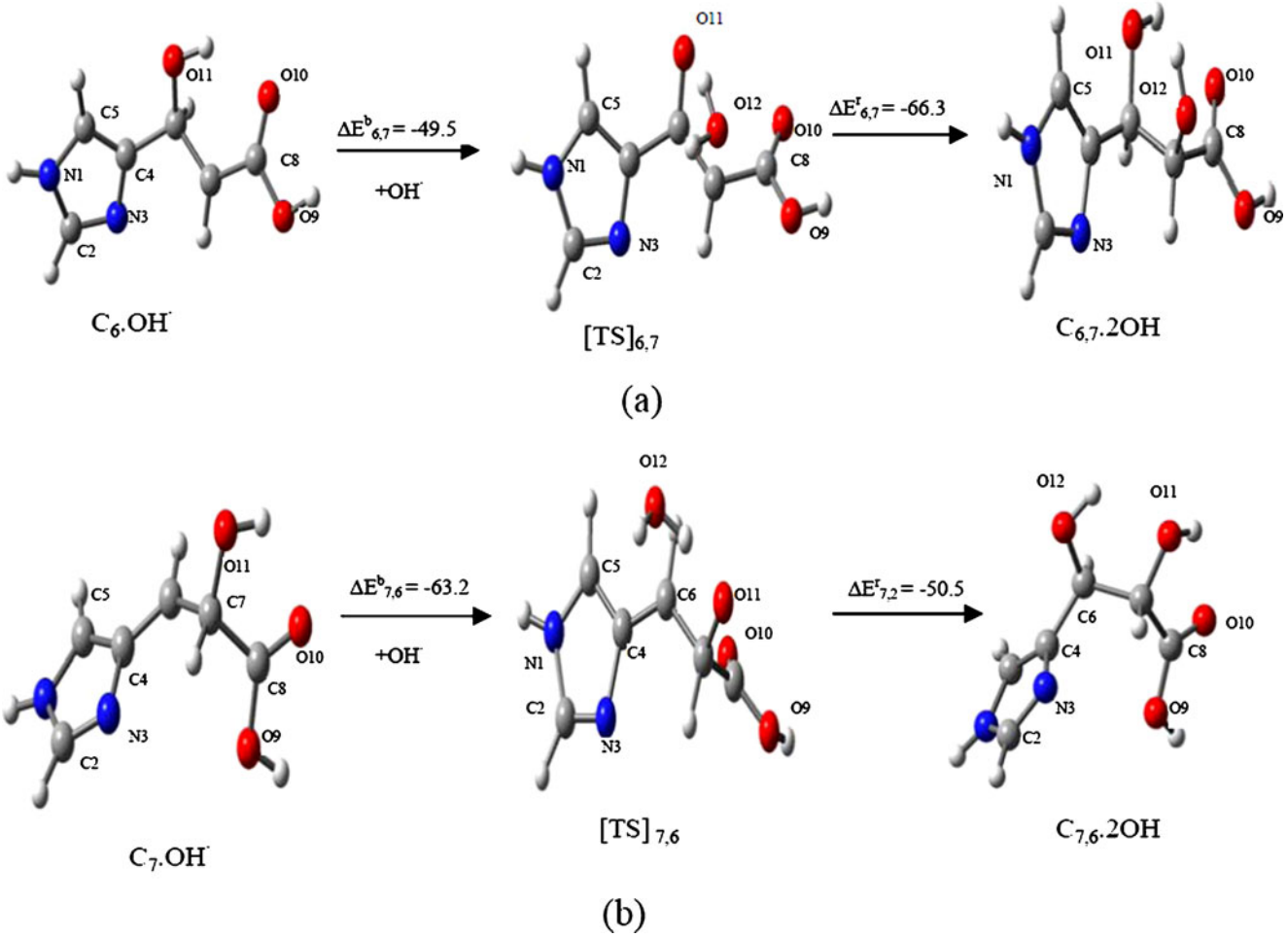

Fig. 3 Addition reactions of the second OH· radical at the **a** C7 position of adduct C_6.OH· and **b** C6 position of adduct C_7.OH·. ZPE- and BSSE-corrected barrier and released energies (kcal mol^{-1}) obtained in aqueous media at the MP2/AUG-cc-pVDZ level of theory using the geometries optimized at the BHandHLYP/AUG-cc-pVDZ level in the gas phase are given near the *arrows*

and also OH bond dissociation, both of which occur barrierlessly, and the corresponding negative barrier energies would get added. Further, consequent to the fourth OH· radical reaction, there is a significant release of energy (23.4 and 37.1 kcal mol^{-1} in Schemes 1 and 2, respectively) (Fig. 4). These released energies would also get added to the negative barrier energies, meaning that the total released energies would be appreciably larger in magnitude than approximately −200 kcal mol^{-1}. The experimentally observed dissociation energy of an OH bond is 117.6 kcal mol^{-1} [74]. Therefore, it is not surprising that the total released energy consequent to a reaction where an OH bond is formed barrierlessly and an OH bond is dissociated barrierlessly is appreciably more than −200 kcal mol^{-1}. In the present work, the changes in Gibbs free energy involved in the reactions of the second, third and fourth OH· radicals, one after the other, are found to be negative, which shows that these reactions are exergonic and would occur spontaneously [75]. In another recent computational study, where the scavenging action of vitamin B6 towards up to eight OH· radicals was studied at the B3LYP/6-31+G** level of theory, the reactions were found to be highly exergonic [76].

Both Scheme 1 and Scheme 2 of the reactions of the third and fourth OH· radicals would operate efficiently, as the reactions are barrierless (Fig. 4). The same product (ImCHO + GLX + 2H_2O) that is also observed experimentally [28] is formed in both schemes. The two products denoted by PC and PC′ in the two schemes differ only with respect to the positions of the water molecules and the relative orientations of the different components. The ZPE-corrected total energies reveal that PC′ is more stable than PC by about 16 kcal mol^{-1} at the BHandHLYP/AUG-cc-pVDZ level of theory in the gas phase, while the corresponding energy difference at the MP2/AUG-cc-pVDZ level in aqueous media is about 8.5 kcal mol^{-1}. These energy differences between PC and PC′ can be understood in terms of the fact that, in PC′, there are four (two strong and two normal) hydrogen bonds, while in PC there are three (one strong and two weak) hydrogen bonds (Fig. 4).

Isospin density surfaces of TS1, IC, TS1′ and IC′ in Schemes 1 and 2 for a spin density value of 0.01 are presented in Fig. 5a, b, e, f, while the corresponding isoelectron density surfaces for the electron density value 0.2e (e = electronic charge) are presented in Fig. 5c, d, g, h, respectively. In TS1 and TS1′, the spin density is localized in the regions involved in the reactions. In IC, the spin density is localized on the GLX moiety, while in IC′ it is localized on the ImCHO moiety. This is easily understood, as the radical character is localized on the GLX moiety in IC while it is localized on the ImCHO moiety in IC′. Thus, spin density distribution is a good indicator of the reactive site. The electron density surfaces of TS1 and TS1′ reveal that the protons that are moving during the reactions carry a Chelpg charge of about 0.3 each. Thus, the protons are positively

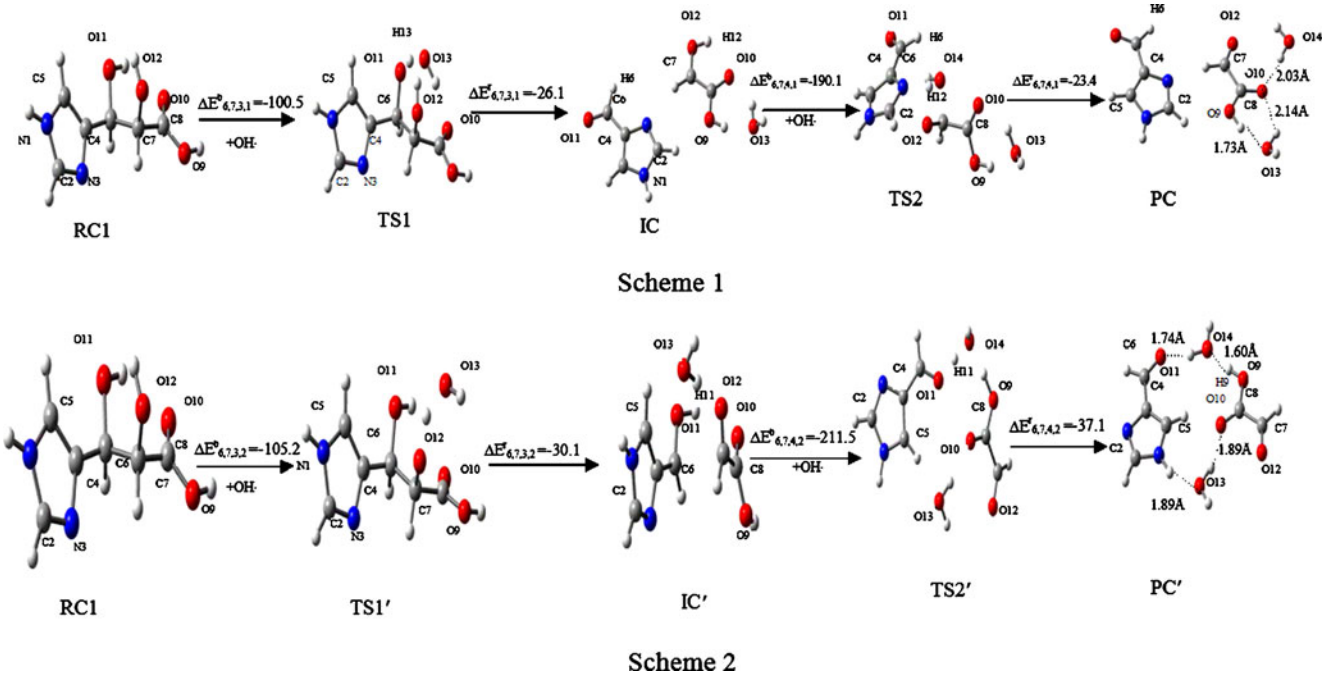

Fig. 4 Reactions of the third and fourth OH· radicals, one after the other, with the $C_{6,7}$.2OH· adduct of UCA. ZPE-corrected barrier and released energies with BSSE correction (except those of $\Delta E_{6,7,4,1}{}^{b}$ and $\Delta E_{6,7,4,1}{}^{b}$, which are not BSSE-corrected) (kcal mol^{-1}) obtained in aqueous media at the MP2/AUG-cc-pVDZ level of theory using the geometries optimized at the BHandHLYP/AUG-cc-pVDZ level in the gas phase are given near the *arrows*

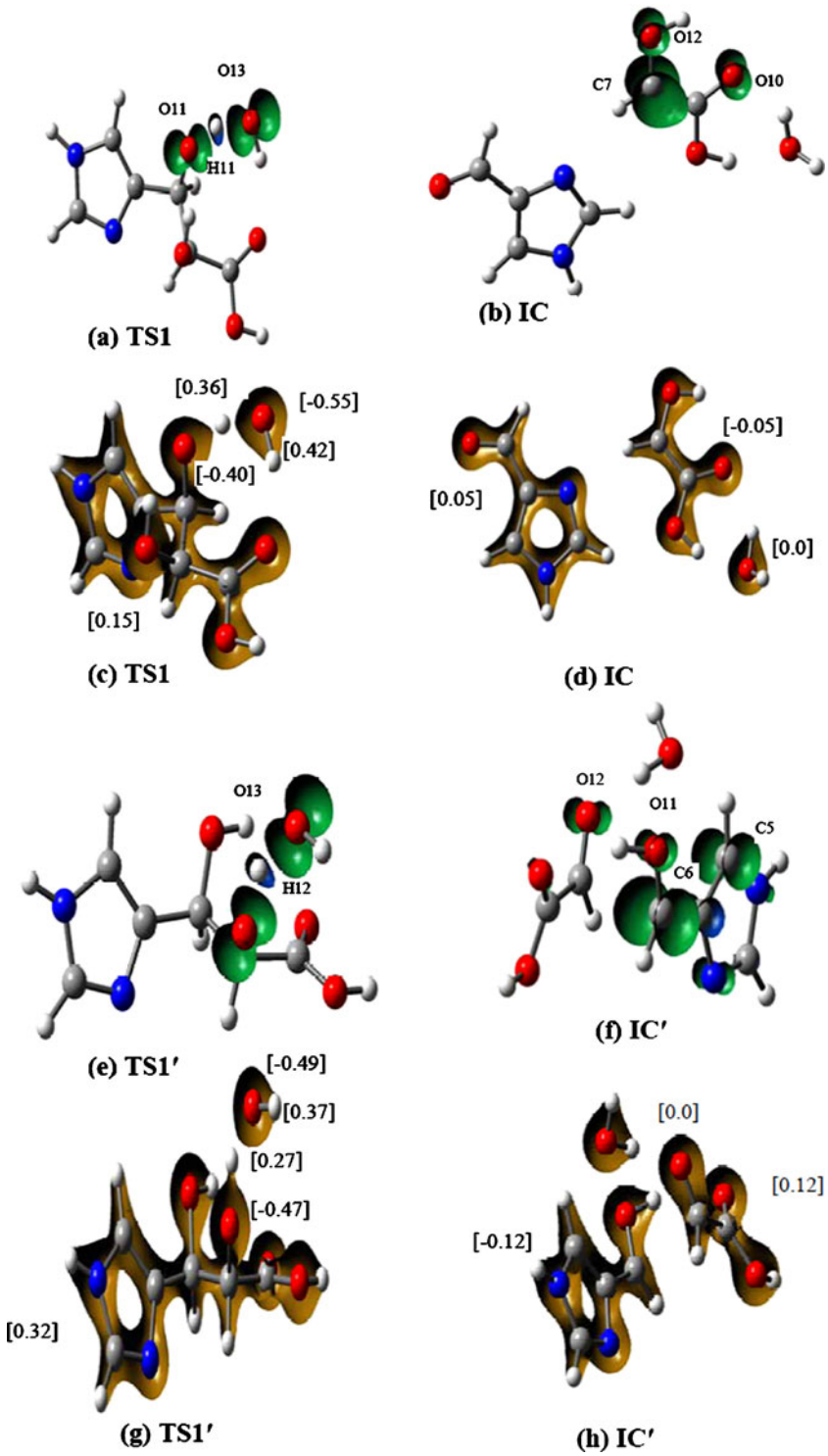

Fig. 5 Spin densities (**a**, **b**, **e**, **f**) and electron density distributions (**c**, **d**, **g**, **h**) in the transition states (TS1) and (TS1′) and intermediate complexes (IC) and (IC′) involved in the reactions of the third radical with the $C_{6,7}$.2OH· adduct of UCA, as shown in Schemes 1and 2 (Fig. 4), obtained at the BHandHLYP/AUG-cc-pVDZ level of theory in the gas phase. Net Chelpg charges obtained at the same level of theory in the gas phase. The surfaces shown in **a**, **b** correspond to the spin density value 0.01, while those shown in **c**, **d**, **e**, **f** correspond to the electron density value 0.2e

charged, as expected, but are still associated with about 70% of their electron density in the isolated atomic state.

A summary of the reaction schemes studied here is presented in Fig. 6. The ZPE- and BSSE-corrected barrier and released energies of the various reaction steps involving one to four OH· radicals, reacting successively, obtained at the MP2/AUG-cc-pVDZ level of theory in aqueous media, are given in this figure. In the summary, the reactions start at the C6 and C7 positions because this is what ultimately leads to the product PC or PC′, which is also observed experimentally. Further, the lowest barrier energies obtained in aqueous media at the MP2/AUG-cc-pVDZ level of theory are given here (Fig. 6). It qualitatively presents the relative positions of the various

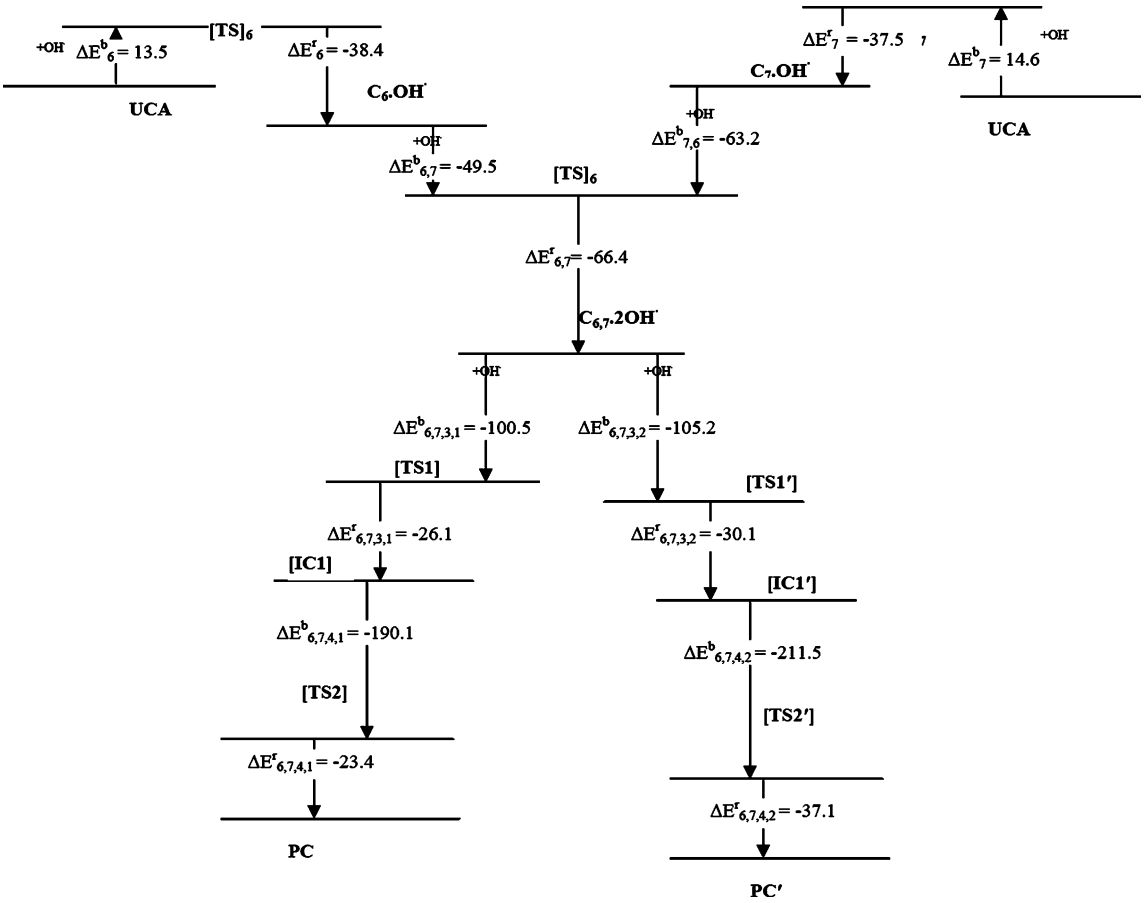

Fig. 6 Summary of the reactions studied here. The various symbols and notations used here have been explained in the text and the other figures. The ZPE- and BSSE-corrected barrier and released energies obtained at the MP2/AUG-cc-pVDZ level of theory in aqueous media are given near the *arrows* ($\Delta E_{6,7,4,1}{}^{b}$ and $\Delta E_{6,7,4,1}{}^{r}$ are not BSSE-corrected)

transition states, intermediates and products in the energy space and clearly shows the barrierless nature of the second to fourth OH· radical reactions. Variations in the ZPE- and BSSE-corrected barrier energies with the number of OH· radicals involved in the reactions are shown in Fig. 7. In plotting this curve, the minimum ZPE- and BSSE-corrected barrier energies involved in one to four OH· radical reactions obtained at the MP2/AUG-cc-pVDZ level of theory in aqueous media were considered. As this curve (Fig. 7) shows, there is near-linear variation in barrier energy (with a negative gradient) with respect to the number of OH· radicals involved in the different reactions.

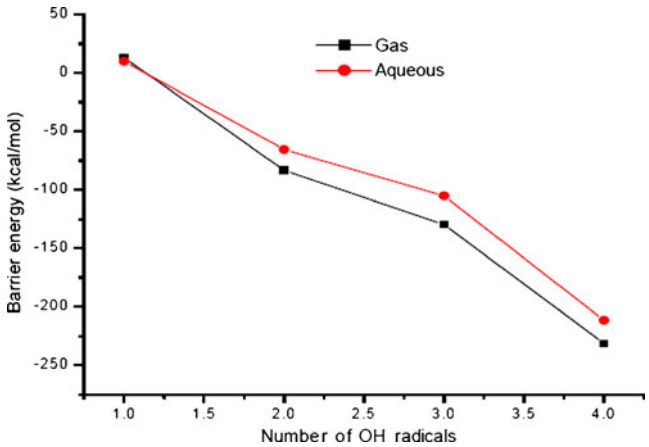

Fig. 7 Variations of ZPE- and BSSE-corrected barrier energies in the gas phase and aqueous media with the number of OH· radicals obtained at the MP2/AUG-cc-pVDZ level of theory using the geometries optimized at the BHandHLYP/AUG-cc–pVDZ level in the gas phase. The lowest barrier energies were considered when plotting this curve

Conclusions

The present study leads us to the following conclusions:

(i) Reactions of UCA with four OH· radicals, one after the other, would lead to the formation of imidazole-4-carboxaldehyde, glyoxylic acid and two water molecules as the primary product. The same product has

also been observed experimentally as the primary product. A positive barrier energy is involved only in the addition reaction of the first OH· radical to UCA, while the reactions of the other three OH· radicals are exergonic. Because of this, UCA would serve as an affective antioxidant, being a good hydroxyl radical scavenger.

(ii) The barrier energy for the isomerization of *trans*-UCA to *cis*-UCA is estimated to be more than 20 kcal mol^{-1}. This is similar to the barrier energy involved in the addition of an OH· radical to UCA at the MP2/AUG-cc-pVDZ level of theory in aqueous media. This shows that the isomerization of *trans*-UCA to *cis*-UCA and reactions of OH· radicals with UCA can occur simultaneously.

Acknowledgments The authors are thankful to the Council of Scientific and Industrial Research (New Delhi) and the University Grants Commission (New Delhi) for financial support.

References

1. Morrison H, Bernasconi C, Pandy G (1984) Photochem Photobiol 40:549–550
2. Norval M, Simpson TJ, Ross JA (1989) Photochem Photobiol 50:267–275
3. Noonan FP, De Fabo EC, Morrison H (1985) J Invest Dermatol 84:342–347
4. Tabachnick J, Weiss C (1959) Rad Result 11:684–699
5. Morrison H (1985) Photodermatology 2:158–165
6. Gibbs NK, Norval M, Traynor M, Wolf BE, Johnson JC (1993) Photochem Photobiol 57:584–590
7. Zenisek A, Kral JA, Hais MI (1955) Biochim Biophys Acta 18:589–591
8. Concar D (1992) New Sci 134:23–28
9. De Fabo EC, Noonan FP (1983) J Exp Med 12:84–98
10. Wille JJ, Kydonieus AF, Murphy GF (1999) Skin Pharmacol Appl Skin Physiol 12:18–27
11. Holan V, Kuffova L, Zajicova A, Krulova M, Filipec M, Holler P, Jancarek AJ (1998) Immunol Today 161:3237–3241
12. Norval M, Gibbs NK, Gilmour J (1995) Photochem Photobiol 62:209–217
13. Noonan FP, De Fabo EC (1992) Immunol Today 13:250–254
14. Higaki Y, Hauser C, Siegenthaler G, Saurat JH (1986) Acta Derm Venereol (Stockh) 66:523–526
15. Noonan FP, De Fabo EC, Morrison HJ (1988) Invest Dermatol 90:92–99
16. Rattis FM, Péguet-Navarro J, Courtellemont, Redziniak G, Schmitt D (1995) Photochem Photobiol 164:65–72
17. Lappin MB, Weiss JM, Schopf E, Norval M, Simon JC (1997) Photodermatol Photoimmunol Photomed 13:163–168
18. Olivarius FF, Dewulf HC, Crosby J, Norval M (1996) Photodermatol Photoimmunol Photomed 12:95–99
19. Shukla MK, Mishra PC (1995) Spectrochim Acta Part A 51:831–838
20. Li B, Hanson KM, Simon JD (1997) J Phys Chem B 101:969–972
21. Hanson KM, Li B, Simon JD (1997) J Am Chem Soc 119:2715–2721
22. Hanson KM, Simon JD (1998) Photochem Photobiol 67:538–540
23. Haralampas GN, Ranson C, Ye T, Rozanaowska M, Wrona M, Sarna T, Simon JD (2002) J Am Chem Soc 124:3461–3468
24. Brookman J, Chacon JN, Sinclair RS (2002) Photochem Photobiol 1:327–332
25. Wendy LR, Levy DH (2001) J Am Chem Soc 123:961–966
26. Ryan WL, Levy DH (2001) J Am Chem Soc 123:961–966
27. Danielsson J, Laaksonen A (2003) Chem Phys Lett 370:625–630
28. Kammeyer A, Eggelte TA, Overmars H, Bootsma JD, Bos JD, Teunissen MBM (2001) Biochim Biophys Acta 1526:277–285
29. Elton LM, Morrison H (2002) Photochem Photobiol 75:565–569
30. Roa R, O'Shea KE (2006) Tetrahedron 62:10700–10708
31. Halliwell B, Gutteridge JMC (1998) Free radicals in biology and medicine, 3rd edn. Oxford University Press, Oxford, p 55
32. Darr D, Fridovich I (1994) J Invest Dermatol 102:671–675
33. Black HS (1987) Photochem Photobiol 46:213–221
34. Gorodetsky R, Sheskin J, Weinreb A (1986) Int J Dermatol 25:440–445
35. Goldblum WR, Derby S, Lerner AB (1953) J Invest Dermatol 20:13–18
36. Aubailly M, Santus R, Salmon S (1991) Photochem Photobiol 54:769–773
37. Boveris A, Oshino N, Chance B (1972) Biochem J 128:617–630
38. Shukla MK, Mishra PC (1996) J Mol Struct 377:247–259
39. Jena NR, Mishra PC (2006) Chem Phys Lett 422:417–423
40. Mishra SK, Mishra PC (2002) J Comput Chem 23:530–540
41. Becke AD (1993) J Chem Phys 98:5648–5652
42. Lee C, Yang W, Parr RG (1998) Phys Rev B 37:785–789
43. Hariharan PC, Pople JA (1972) Chem Phys Lett 66:217–219
44. Becke AD (1988) Phys Rev 38:3098–3100
45. Schoone K, Smets J, Houben L, Van Bael MK, Adamowicz L, Maes G (1998) J Phys Chem A 102:4863–4877
46. Cossi M, Scalmani G, Regga N, Barone V (2002) J Chem Phys 117:43–54
47. Miertus S, Tomasi (1982) J Chem Phys 65:239–245
48. Miertus S, Scrocco E, Tomasi (1981) J Chem Phys 55:117–129
49. Møller C, Plesset MS (1934) Phys Rev 46:618–622
50. Frisch MJ, Head-Gordon M, Pople JA (1990) Chem Phys Lett 166:275–280
51. Woon DE, Dunning TH Jr (1993) J Chem Phys 98:1358–1371
52. Boys SF, Bernardi F (1970) Mol Phys 19:553–566
53. Simon S, Duran M, Dannenberg JJ (1996) J Chem Phys 105:11024–11031
54. Frisch MJ, Trucks GW, Schlegel HB, Scuseria GE, Robb MA, Cheeseman JR, Zakrzewski VG, Montgomery JA Jr, Stratmann RE, Burant JC, Dapprich S, Millam JM, Daniels AD, Kudin KN, Strain MC, Farkas O, Tomasi J, Barone V, Cossi M, Cammy R, Mennucci B, Pomelli C, Adamo C, Clifford S, Ochterski J, Petersson GA, Ayala PY, Cui Q, Morokuma K, Rega N, Salvodar P, Dannenberg JJ, Malick DK, Rabuck AD, Raghavachari K, Foresman JB, Cioslowski J, Ortiz JV, Baboul AG, Stefanov BB, Liu G, Liashenko A, Piskorz P, Komaromi I, Gomperts R, Martin RL, Fox DJ, Keith T, Al-Laham MA, Peng CY, Nanayakkara A, Challacombe M, Gill PMW, Johnson B, Chen W, Wong MW, Andres JL, Gonzalez C, Head-Gordon M, Replogle ES, Pople JA (2001) Gaussian 98, Revision A.11.2. Gaussian Inc., Pittsburgh
55. Frisch AE, Dennington RD, Keith TA, Neilsen AB, Holder AJ (2003) GaussView, Rev 3.9. Gaussian Inc., Pittsburgh
56. Danielsson J, Uličný J, Laaksonen A (2001) J Am Chem A 123:9817–9821
57. Tiwari S, Mishra PC, Suhai S (2007) Int J Quantum Chem 108:1004–1016
58. Tiwari S, Mishra PC (2009) Spectrochim Acta Part A 73:719–729
59. Lahti A, Hotokka M, Neuvonen K, Ayras P (1997) Struct Chem 8:331–342

60. Lahti A, Hotokka M, Neuvonen K, Ayras P (1995) J Mol Struct Theochem 331:169–179
61. Lahti A, Hotokka M, Neuvonen K, Karlstrom G (1999) Int J Quantum Chem 72:25–37
62. Page CS, Merchán M, Serrano-Andres L, Olivucci M (1999) J Phys Chem A 103:9864–9871
63. Danielsson J, Söderhäll A, Laaksonen A (2002) Mol Phys 100:1873–1886
64. Page CS, Olivucci M, Merchán M (2000) J Phys Chem A 104:8796–8805
65. Hawkinson SW (1977) Acta Cryst 33:2288–2294
66. Jeffrey CG, Lubos M (1997) Phys Rev Lett 79:4353–4357
67. Ghigo G, Tonachini G (1999) J Chem Phys 110:7298–7304
68. Glukhovtsev MN, Bach R, Pross A, Radom LJ (1996) Chem Phys Lett 260:558–564
69. Jena NR, Mishra PC (2005) J Phys Chem B 29:14205–14218
70. Tiwari S, Shukla PK, Mishra PC (2008) J Mol Model 14:631–640
71. Szori M, Fittschen C, Csizmadia IG, Viskolcz B (2006) J Chem Theory Comput 2:1575–1586
72. Chen X, Zhan CG (2004) J Phys Chem A 108:3789–3791
73. Kammeijer A, Bos JD (2006) US Patent 7056938
74. Chadra AK, Uchimaru T (2002) Int J Mol Sci 3:407–422
75. McNaught A, Wilkinson A (1997) IUPAC compendium of chemical terminology, 2nd edn. Blackwell, Oxford
76. Mataxain JM, Padro D, Ristilla M, Strid A, Eriksson LA (2009) J Phys Chem Lett B 113:9629–9632